Quantitative Characterization of Three-Dimensional Damage Evolution in a Wrought Al-Alloy under Tension and Compression

H. AGARWAL, A.M. GOKHALE, S. GRAHAM, and M.F. HORSTEMEYER

Three-dimensional (3-D) microstructural damage due to cracking of Fe-rich intermetallic particles is quantitatively characterized as a function of strain under compression and tension in an Al-Mg-Si base wrought alloy. The 3-D number fraction of damaged (cracked) particles, their average volume, average surface area, and shape factor are estimated at different strain levels for deformation under uniaxial tension and compression. It is shown that, depending on the type of loading, loading direction, particle shape, and microstructural anisotropy, the two-dimensional (2-D) number fraction of the damaged particles can be smaller or larger than the corresponding true 3-D number fraction. Under uniaxial tension, the average volume and surface area of cracked particles decrease with the strain. However, the average volume and surface area of the cracked particles *increase* with the increase in the compressive strain, implying that more and more larger elongated particles crack at higher and higher stress levels, which is contrary to the predictions of the existing particle cracking theories. In this alloy, the damage development due to particle cracking is intimately coupled with the particle rotations. The differences in the damage evolution under tension and compression are explained on the basis of the differences in the particle rotation tendencies under these two loading conditions.

I. INTRODUCTION

FAILURE of numerous ductile materials involves cracking of second-phase inclusions/particles, growth of microvoids at the cracks in the damaged particles, and microvoid coalescence. Therefore, to understand the damage evolution and fracture processes in such materials, it is of interest to quantitatively characterize particle cracking as a function of strain under different loading conditions. It must be recognized that the microstructural damage (such as particle cracking) is of three-dimensional (3-D) nature. In general, important attributes of the 3-D microstructural damage such as number fraction of cracked particles, their average volume, surface area, *etc.* cannot be estimated from any measurements performed on independent random two-dimensional (2-D) sections through the 3-D microstructure.[1–4] Nonetheless, in all the earlier studies, characterization of particle cracking has been performed only in independent random 2-D metallographic planes through the 3-D microstructural space. Further, a majority of the earlier investigations focus on the damage evolution under uniaxial tensile stress.[5–8] Damage evolution under other test conditions (for example, under compression, torsion, *etc.*) has received very little attention. To the best of the authors' knowledge, cast A356 Al-alloy is the only material in which the damage evolution (cracking and debonding of Si particles) has been quantitatively characterized under tension, compression, and torsion,[9,10] and as a function of temperature[11] and strain rate.[12]

H. AGARWAL, Process Engineer, is with Intel Corporation, Santa Clara, CA 95052. A.M. GOKHALE, FASM, Professor, is with the School of Materials Science and Engineering, Georgia Institute of Technology, Atlanta, GA 30332-0245. Contact e-mail: arun.gokhale@mse.gatech.edu S. GRAHAM, Senior Member of Technical Staff, and M.F. HORSTEMEYER, Manager, are with the Sandia National Laboratories, Livermore, CA 94551-0969.

Manuscript submitted May 9, 2001.

The objective of this contribution is to quantitatively characterize the evolution of 3-D microstructural damage due to cracking of Fe-rich intermetallic inclusions in 6061 aluminum alloy under uniaxial tension and compression. The 3-D number fraction, volume fraction, total surface area per unit volume, average volume, and average surface area of the cracked Fe-rich particles are estimated as a function of strain under uniaxial compression and tension by using 2-D and 3-D stereological probes and digital image analysis techniques. It is observed that there are significant differences in the particle cracking damage development under tension and compression. The experimental data show that, depending on the loading condition, strain level, microstructural anisotropy, and particle shape, significant *rotations* of the Fe-rich particles occur during plastic deformation of the matrix. These particle rotations in turn affect the particle cracking process by bringing the new particles in the morphological orientations that facilitate particle cracking. The differences in the damage evolution under tension and compression are explained on the basis of the particle rotations.

II. EXPERIMENTAL

A. *Materials*

The experiments were performed on the specimens drawn from an extruded round bar (88-mm diameter) of 6061 Al-alloy (T651 condition) supplied by ALCOA. The chemical composition of the alloy is given in Table I.

B. *Mechanical Tests*

In the extruded Al-alloy bar stock, microstructural and/or chemical gradients may exist in the radial direction. To ensure that the test specimens have statistically similar

Table I. Chemical Composition of 6061 Al-Alloy

Element	Zn	Ti	Si	Mn	Mg	Fe	Cu	Cr	Al
Wt pct	0.02	0.01	0.65	0.04	1.06	0.37	0.28	0.2	balance

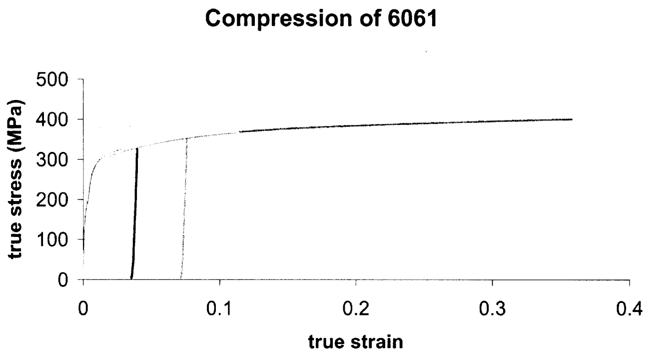

Fig. 1—Stress-strain curve of 6061 Al-alloy under uniaxial compression.

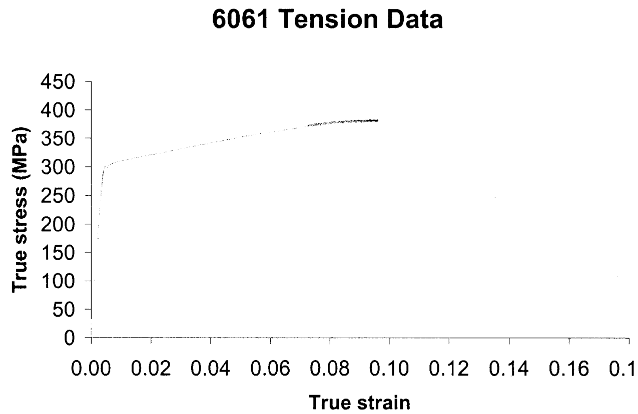

Fig. 2—Stress-strain curve of 6061 Al-alloy under uniaxial tension.

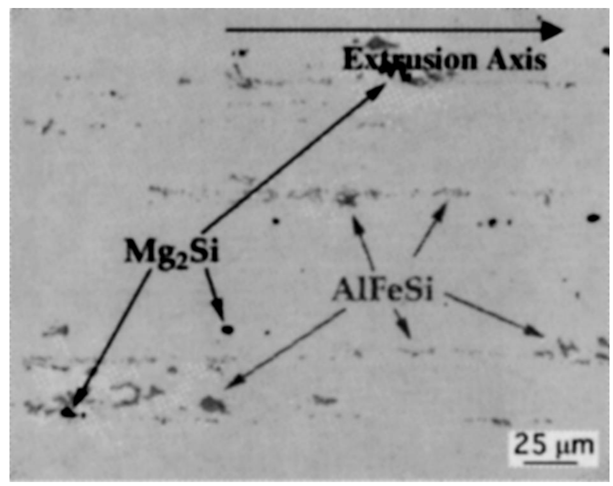

Fig. 3—Microstructure of unstrained 6061 Al-alloy.

microstructure and the same alloy chemistry, all the specimens were extracted from the bar stock at a radial distance of 20 mm from the bar center. For all the mechanical tests, the loading direction was parallel to the extrusion axis.

An axial-torsional servohydraulic test frame (MTS81) was used for the compression tests. The quasi-static uniaxial compression tests were performed on cylindrical specimens of 9-mm diameter and 12.5-mm length at the strain rate of 2×10^{-4} per second. Concentric grooves were machined into the ends of the specimens in which a Mo-based lubricant was placed. The lubrication was necessary to ensure homogeneous deformation of the specimens. The specimens were examined at the end of each test; no barreling effects were seen. Thus, homogeneous deformation conditions can be assumed for the compression tests. These quasi-static tests were interrupted at different strain levels to study the particle cracking phenomena as a function of strain. Figure 1 shows compression true stress–true strain curve for the specimens under present investigation.

The uniaxial tensile tests were performed on an MTS 880 servohydraulic test frame. The tensile test specimens were of 6.25-mm diameter and 25-mm length. The tensile tests were preformed in a displacement-controlled mode at the displacement rate of 5×10^{-3} mm per second. In order to study the progression of the damage, a series of interrupted tensile tests were performed at different strain levels. Figure 2 shows uniaxial true stress–true strain curve for the specimens under present investigation.

C. *Metallography*

The specimens were cut in the center along vertical planes containing the applied load direction, which is also the extrusion axis of extruded bar. The specimens were mounted and then polished by using standard metallographic techniques. The specimens were observed under optical microscope in unetched condition. Figure 3 shows a typical microstructure of an unstrained specimen in unetched condition. Observe that the microstructure contains two types of particles in the aluminum matrix. Light gray particles are Fe-based intermetallics, and the dark particles are Mg_2Si intermetallics. Note that both type of particles are mostly oriented parallel to the extrusion axis, which is also the loading direction for all the specimens. Thus, the extrusion axis/loading direction is the axis of microstructural anisotropy. Figure 4 depicts the microstructure of a deformed specimen showing cracked Fe-rich intermetallic particles. In 6061 Al-alloy, the damage due to cracking of Mg_2Si intermetallics is observed to be negligible in comparison to that due to cracking of Fe-based intermetallics. Therefore, in the present study, cracking of only the Fe-rich intermetallics has been quantitatively characterized. The cracked Fe-rich particles have been detected *via* the contrast resulting from the separation of the two associated crack traces observed in the cracked particles. It follows that only those cracks (and, therefore, cracked particles) having crack separation larger than the resolution limit of the optical microscope ($\sim$0.5 μm) can be detected in this manner. Therefore, a cracked particle is detected at a strain level somewhat higher than the strain at which the crack was formed.

D. *Quantitative Metallography*

The number density, volume fraction, and total surface area per unit volume of cracked Fe-rich particles were measured at different compressive and tensile strain levels. These

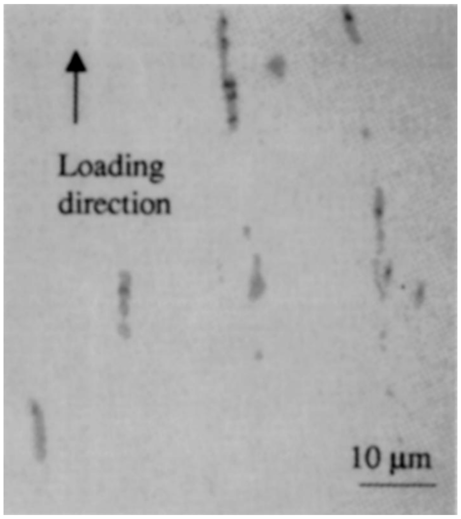

(*a*)

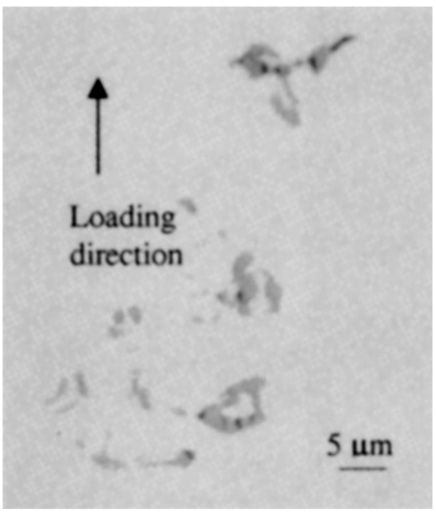

(*b*)

Fig. 4—Microstructures of strained specimens showing cracked Fe-rich intermetallic particles. (*a*) Particle cracks in the specimen strained to 0.107 tensile strain level. These cracks are almost *perpendicular* to the loading direction. (b) Particle cracks in the specimen strained to 0.70 compression strain level. These cracks are almost *parallel* to the loading direction.

measurements were performed on a large number of contiguous fields, typically, around 350 to 400 fields, to avoid edge effects in the damage quantification. To measure the size and shape of a cracked particle by image analysis, the crack is filled-in using the image editing techniques. Therefore, the measured size and shape of the cracked particles pertain to their values in the undamaged state. All the measurements were averaged out over the entire specimen in order to average over any microstructural gradients.

Volume fraction of the cracked Fe-rich particles was estimated by using standard stereological techniques.[3,4] As the microstructure is anisotropic, design-based stereological sampling is essential for unbiased and efficient estimation of the total surface area of the damaged Fe-rich particles per unit volume of microstructure. These measurements were carried out by using the design-based stereological technique that involves counting the number of intersections between particle boundaries and approporately oriented *cycloid shaped test lines* placed on vertical metallographic sections.[13,14] In the present case, the microstructural anisotropy is symmetric with respect to the loading direction (which is also the extrusion axis), and, therefore, such measurements on a vertical plane of any one orientation containing the loading direction yield an efficient and unbiased estimate of the 3-D total surface area of the damaged Fe-rich intermetallic particles per unit volume, when loading direction is chosen as the vertical axis.[13]

It is well known that,[1–4] in general, the 3-D number density of particles cannot be estimated from any measurements performed on independent random 2-D metallographic sections. Estimation of 3-D number density requires sampling of 3-D microstructure by using a 3-D test probe. The number density of particles in 3-D microstructure can be estimated by unbiased counting of particles in 3-D microstructural space by using a pair of planes at random locations, and following either the disector[15] or the large area disector[16] methodology. The disector method (as well as large area disector method) involves use of a 3-D stereological probe consisting of a pair of planes that are a known distance apart. The particles that appear in the first section but are *not* present in the second section are counted (let this number be Q^-). Similarly, the particles that are *not* present in first plane, but are present in the second, are also counted (let this number be Q^+). The estimate of the number of these features per unit volume, N_V, is given by the following relationship:[15]

$$N_V = [Q^+ + Q^-]/[2 \cdot A \cdot h] \qquad [1]$$

where h is the distance between the disector planes and A is the area of the disector.

In the present study, large area disector (LAD) methodology has been adopted, as it is very efficient as well as unbiased.[16,17] The distance between two consecutive LAD planes was kept 1 μm (one-fifth of the particle average size). Three sets of LADs were analyzed to get the 3-D number density of intermetallic particles in each specimen. First, a montage of contiguous 2-D images was grabbed on the first metallographic plane using the image analysis technique developed by Louis and Gokhale.[18] The specimen was then polished to remove 1-μm thickness of the material. The amount of material removed was controlled by monitoring the diagonal length of microhardness diamond indents. A 2-D montage was then grabbed on the second metallographic plane exactly at the same position as the first one. The LAD planes were aligned by using the locations of the microhardness indents for reference. The thickness of material removed (*i.e.*, distance between the LAD planes, h) was calculated by measuring the difference in the diagonal length of the diamond indents in the two LAD planes and the apex angle and geometry of the microhardness indentor.

III. RESULTS AND DISCUSSIONS

A. *Damage Evolution in Compression*

The average volume (or average surface area) of cracked Fe-rich intermetallic particles can be calculated by dividing the experimentally measured volume fraction (or total surface area per unit volume) of the cracked intermetallic particles by their 3-D number density measured by the LAD technique. The particle shape factor Ω can be estimated from

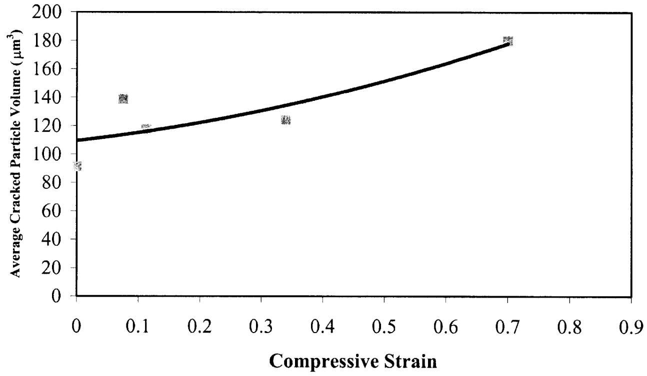

Fig. 5—Plot of average cracked particle volume *vs* true compressive strain.

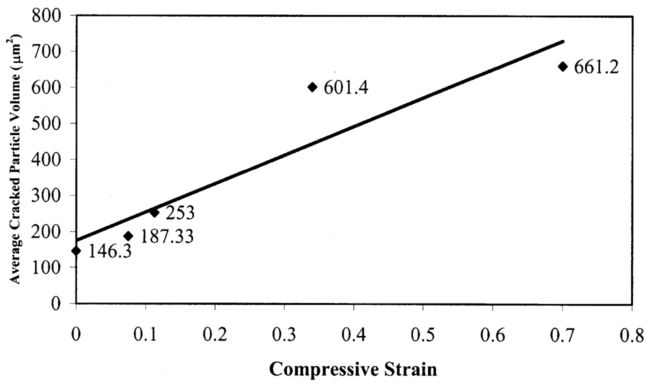

Fig. 6—Plot of average cracked particle surface area *vs* true compressive strain.

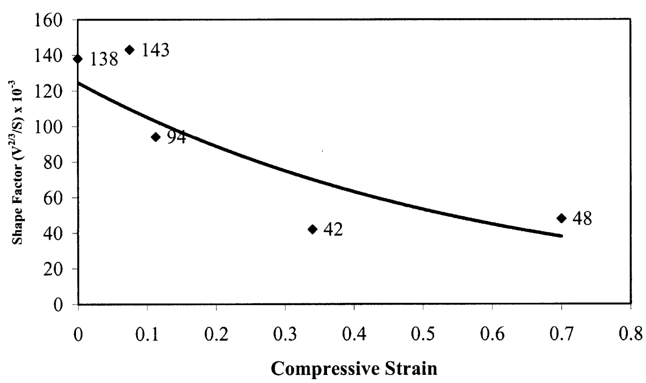

Fig. 7—Plot of average cracked particle shape factor *vs* true compressive strain.

the average cracked particle volume V_c and average cracked particle surface area S_c as follows:

$$\Omega = [V_c]^{2/3}/[S_c] \qquad [2]$$

For equiaxed particle shapes (such as sphere), Ω is equal to 0.21 (*i.e.* $[1/36\pi]^{1/3}$), and it decreases as the particles become more and more elongated.

Figures 5 through 7 report the variation of *average* cracked particle volume (not the volume fraction), *average* surface area (not the total surface area per unit volume), and their shape factor Ω as a function of compressive strain, respectively. In these plots, the attributes corresponding to zero strain level are those for overall bulk Fe-rich intermetallic particle population in the unstrained specimen. Observe that both average volume and average surface area of the cracked Fe-rich intermetallic particles *increase* with the increase in the compressive strain (Figures 5 and 6), whereas the shape factor Ω *decreases* with the increase in the compressive strain (Figure 7). As the average cracked particle volume and surface area increase with the strain, it implies that more and more *larger* particles must crack at higher and higher compressive strain levels. Similarly, for the shape factor Ω to decrease with the strain, more and more elongated particles must crack at higher and higher strain levels. However, according to almost all theoretical and experimental studies on particle cracking,[1,2,5–12,19–22] the larger and elongated particles have a higher probability of cracking because the critical tensile stress required for cracking is lower for larger particles. Gurland and Plateau[8] have given the following equation for critical tensile stress σ to develop a crack in a particle of size D.

$$\sigma = [E\gamma/(Dq^2)]^{1/2} \qquad [3]$$

In Eq. [3], q is the stress concentration factor at the particle, E is weighted average of the elastic moduli of the particle and matrix, and γ is the interfacial energy of the crack. Thus, the stress σ required to crack a particle is inversely proportional to the square root of the particle size, and, therefore, larger particles crack at lower stresses. It follows that, as the damage accumulates, the largest particles are expected to fracture at lowest stress levels, and progressively smaller and smaller particles may crack at higher and higher stress levels. Due to such damage accumulation, the average volume and average surface area of the cracked particles must *decrease* with the increase in the strain, which is the *opposite* of what is observed experimentally (Figures 5 and 6).

It is also well known that[5–8] elongated particles are expected to crack at lower stresses. Therefore, if the microstructure contains an ensemble of particles of different shapes and sizes, large elongated particles are expected to crack at lowest stress levels, and progressively smaller and equiaxed particles may crack at higher and higher stress levels. In such a case, the shape factor Ω should increase with the increase in the applied stress, which is also the *opposite* of what is observed experimentally (Figure 7).

Due to thermomechanical processing of the alloy, the Fe-rich intermetallic particles have preferred orientations: the majority of these particles have their longest dimension parallel (or almost parallel) to the extrusion axis (Figure 3), which is the loading direction. The morphological anisotropy of the particles has an effect on the probability of particle cracking. The particle cracking is expected to depend significantly on the maximum principal tensile stress component, which is largest in the direction *perpendicular* to the loading direction for the *compression* test specimens. Therefore, the elongated particles, whose major axis is parallel to the induced tensile stress, have significantly higher probability of fracture, as compared to the particles that are aligned perpendicular to the induced tensile stress direction (*i.e.*, parallel to the loading axis/extrusion direction). In the present microstructure, only a small percentage of the Fe-rich intermetallic particles have their major axis parallel to the induced tensile stress direction.

Figure 8 shows the morphological orientation distribution

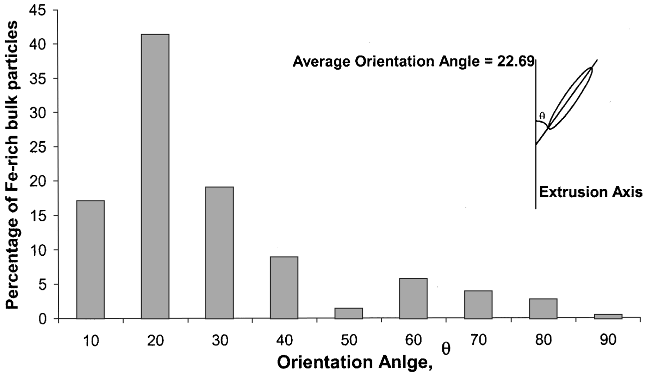

Fig. 8—Morphological orientation distribution of Fe-rich bulk intermetallic particles in an unstrained specimen.

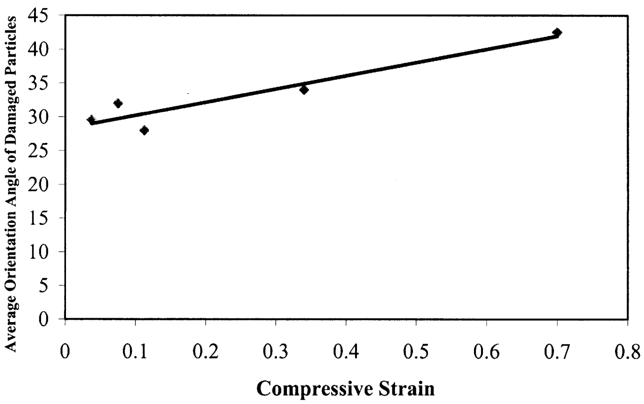

Fig. 9—Variation of average orientation angle of the damaged particles with compressive strain.

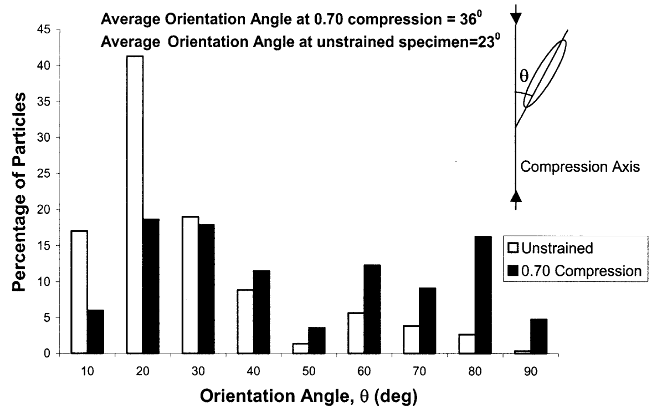

Fig. 10—Comparison of morphological orientation distribution of Fe-rich bulk intermetallic particles in unstrained specimen and the specimen deformed to 0.70 compressive strain.

of the major axis of the Fe-rich intermetallic particles in an *unstrained* specimen. In this figure, the orientation of a particle is given by the angle between the major axis of the particle and the extrusion axis, which is the also the loading direction for the compression test specimens. Observe that 77 pct of the particles have their major axis at an angle between 0 and 30 deg with the extrusion axis, whereas only about 7 pct of the particles have their major axis oriented at an angle between 60 and 90 deg with respect to the extrusion axis. Large and elongated particles having orientations in this range (*i.e.*, 60 to 90 deg) are most likely to crack at lowest stress (or strain) levels. The particles in other orientations may crack at higher stress (strain) levels. Such damage progression should lead to a *decrease* in the average orientation angle of the *cracked particles* with an increase in the applied compressive stress (or strain). However, the experimental data presented in Figure 9 show that the average orientation angle of the cracked particles *increases* with the strain.

To explain the paradoxical behavior of the experimental data on average volume (and surface area) of the cracked particles, their shape, and orientations, recall that all current theories of particle cracking and damage initiation[5–8,19–22] implicitly assume that the particles are *stationary* in the 3-D microstructural space, and, therefore, do not undergo any rotations when a stress is applied. All the experimental observations can be logically explained if significant particle rotations occur under an applied stresses. Therefore, it is of interest to determine if the overall particle population undergoes any rotations as the matrix is plastically deformed. For this purpose, the morphological orientation distribution function of the overall Fe-rich intermetallic particle population (cracked and uncracked) was experimentally measured in different specimens using digital image analysis. Figure 10 compares the orientation distribution of the bulk Fe-rich particles in the unstrained specimen with the corresponding distribution in the 0.70 compression strain specimen (note that this distribution includes both undamaged and cracked particles). As mentioned earlier, in the unstrained specimen, 77 pct of the particles have their orientation angles between 0 and 30 deg, and only 7 pct have their orientation angle between 60 and 90 deg. On the other hand, in the specimen strained to 0.70 compression strain, about 43 pct of the particles have their orientations in the range of 0 to 30 deg, and 30 pct of the particles are oriented at angles in the range of 60 to 90 deg with respect to the loading direction. In other words, the percentage of the particles in the orientation range 60 to 90 deg in the bulk population (damaged and undamaged) has increased from 7 to 30 pct when the specimen is strained to 0.70 strain level in compression. Further, the average orientation angle of the (damaged and undamaged) Fe-rich particles has increased from 24 deg in the unstrained specimen to 36 deg in the specimen with 0.70 compressive strain. Note that these orientation data have been obtained by measuring orientations of about 5000 particles in each specimen, and, therefore, the data are robust. These data clearly demonstrate that the brittle Fe-rich intermetallic particles rotate during the plastic deformation of the specimens under compressive load, and they tend to align themselves along the direction perpendicular to the loading axis, which is the direction of the induced tensile stress. Therefore, these particle rotations bring *new* particles in the orientations that facilitate further cracking. Consequently, at higher and higher strains, *new* larger and elongated particles are brought in the orientations that facilitate particle cracking, which should lead to an increase in the average particle volume and average orientation of damaged particles, as observed experimentally (Figures 5 through 8).

The joint bivariate size and morphological orientation data (Figure 11) bring out another interesting observation. In the unstrained specimen, the average major axis of the bulk Fe-rich intermetallic particles (*i.e.*, damage and undamaged) having orientations in the range of 60 to 90 deg is 3.7 μm, whereas in the 0.70 compression strain specimen, the average major

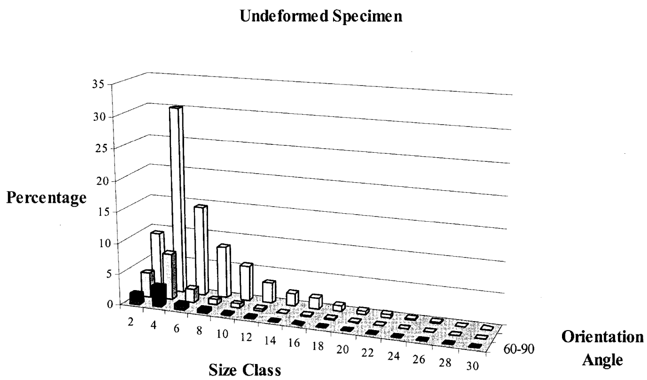

(*a*)

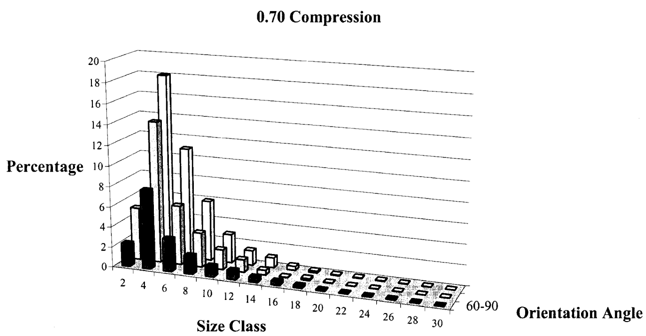

(*b*)

Fig. 11—Bivariate size and orientation distribution of Fe-rich damaged intermetallic particles in the 0.70 compression strain specimen.

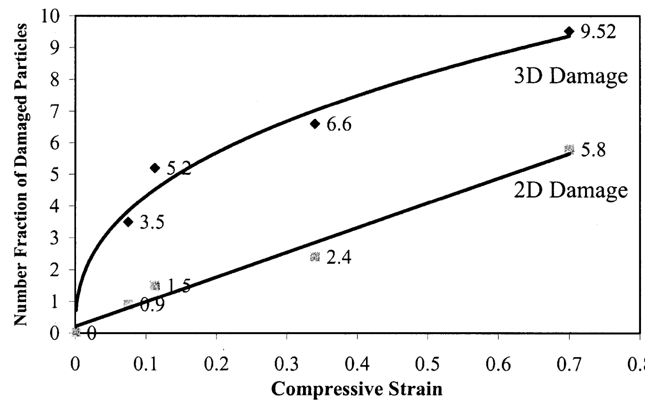

Fig. 12—Variation of 2-D and 3-D number fraction of Fe-rich damaged intermetallic particles with respect to compressive strain.

axis of the bulk particles in the same orientation range is 5.1 μm. In other words, the average size of the particles that are perpendicular or almost perpendicular (*i.e.*, 60 to 90 deg orientations) to the loading direction (*i.e.*, parallel to induced tensile stress direction) has increased by about 40 pct as a result of 0.70 uniaxial compressive strain along the direction parallel to the extrusion axis. One possible explanation is that a greater number of larger particles rotate as compared to smaller ones, leading to an increase in the number fraction of the larger particles in the orientation range (60 to 90 deg) that facilitates particle cracking. Consequently, the average volume, surface area, and orientation angle of damaged particles increase with strain. Further, in the unstrained specimen, most of the larger particles are also the most unequiaxed (elongated) ones; therefore, the shape factor of the damaged particles also decreases with the compressive strain.

Figure 12 shows a plot of number fraction f of broken/cracked Fe-rich intermetallic particles observed in a representative metallographic plane (2-D) containing the loading direction, as well as number fraction F of cracked/broken Fe-rich particles in 3-D microstructural space, as a function of strain under uniaxial compression. As expected, both the 2-D and 3-D damage descriptors increase with the strain. However, the 3-D damage parameter F is *larger* than the 2-D damage parameter f at each strain level in uniaxial compression.

It is well known that[3,4] the probability that a given particle intersects a sectioning plane is directly proportional to the size (or, strictly speaking, caliper diameter) of the particle in the direction perpendicular to the sectioning plane. Therefore, for the same 3-D number density of the particles, their 2-D number density can decrease with the decrease in the average size in the direction perpendicular to the sectioning plane. In the present microstructure, the particles have anisotropic orientations, and larger elongated and thin particles fracture more frequently (and also rotate preferentially) as compared to equiaxed and thick particles. Therefore, the average dimension of the cracked particles in the direction perpendicular to the vertical metallographic plane is expected to be lower than the corresponding average dimension of the overall bulk particle population. Therefore, on the average, the probability of a cracked particle intersecting the chosen metallographic plane is less than the corresponding average probability for the overall bulk particle population. Consequently, the fraction of cracked particles observed on the chosen metallographic plane in a given specimen should be lower than the true 3-D number fraction of cracked particles F, which is also observed experimentally at each strain level in compression. It is important to point out that this behavior arises only due to nonequiaxed shapes of the particles in the bulk microstructure, and the microstructural anisotropy that tends to align the major axis of the particles parallel to the extrusion axis. If the same particles were of spherical shape, and larger particles crack preferentially, then, on the average, the probability of the cracked particles intersecting the metallographic plane would be larger than the corresponding average probability for the overall bulk particle population. In such a case, the 2-D number fraction of cracked particles would be higher than the corresponding 3-D number fraction. Therefore, depending on the type of loading, loading direction, particle shape, and microstructural anisotropy, the 2-D number fraction of the damaged particles can be smaller or larger than the corresponding 3-D number fraction of the damaged particles.

E. *Damage Evolution in Tension*

Figures 13 and 14 show the variation of average volume and average surface area of damaged (cracked/broken) Fe-rich intermetallic particles with strain under uniaxial tension, respectively. Observe that both average volume and average surface area of damaged Fe-rich intermetallic particles *decrease* with the strain under uniaxial tension (which is the opposite of the trend observed in the compression test specimens). Figure 15 shows a plot of variation of damaged Fe-rich intermetallic particle shape factor with strain in the tensile test specimens. The plot reveals that as the strain increases, the particle shape factor increases (which is also the opposite of the trend observed in the compression test

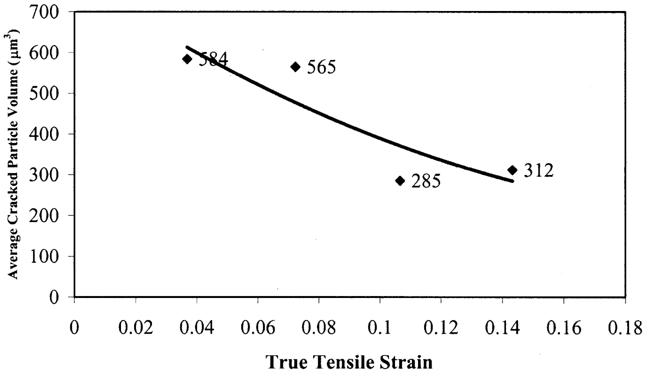

Fig. 13—Variation of average Fe-rich damaged intermetallic particle volume with true tensile strain.

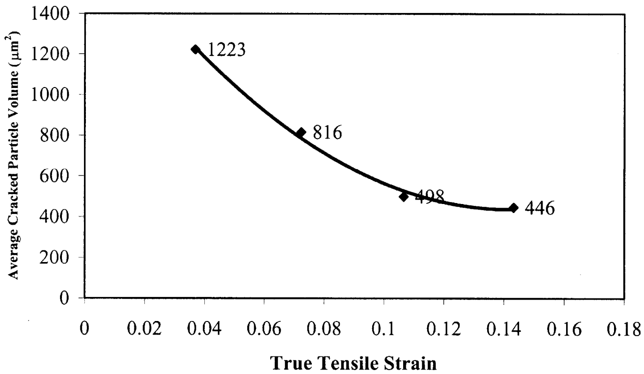

Fig. 14—Variation of average Fe-rich damaged particle surface area with true tensile strain.

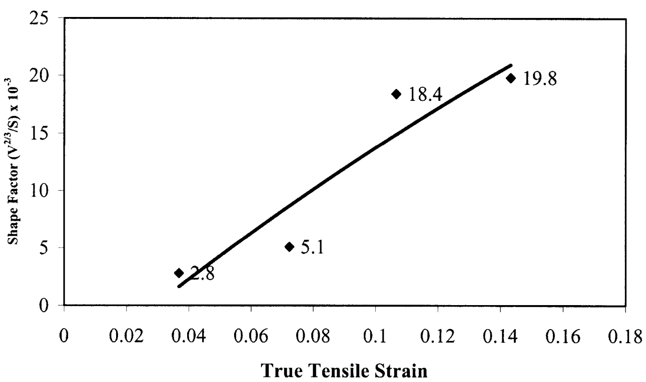

Fig. 15—Variation of shape factor of Fe-rich damaged particles with true tensile strain.

specimens). These data reveal that smaller and equiaxed particles tend to crack at high levels of tensile strain, whereas larger particles crack at low strains, as one would expect, if there are no significant particle rotations. Under the tensile stress, the particles are expected to rotate to align themselves parallel to the applied tensile stress direction, which is the extrusion axis of the specimens under investigation. In the unstrained specimen, most of the particles are already aligned parallel to the extrusion axis, and due to that, no significant changes in the morphological orientation distribution are expected in the tensile test specimens due to particle rotations. Significant particle rotations would have

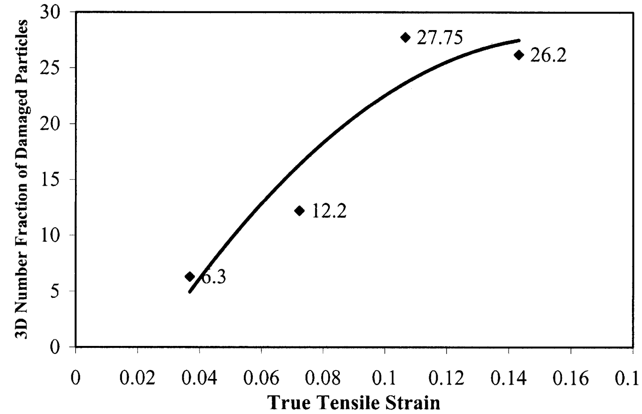

Fig. 16—Plot of 3-D number fraction of Fe-rich damaged particles *vs* true tensile strain.

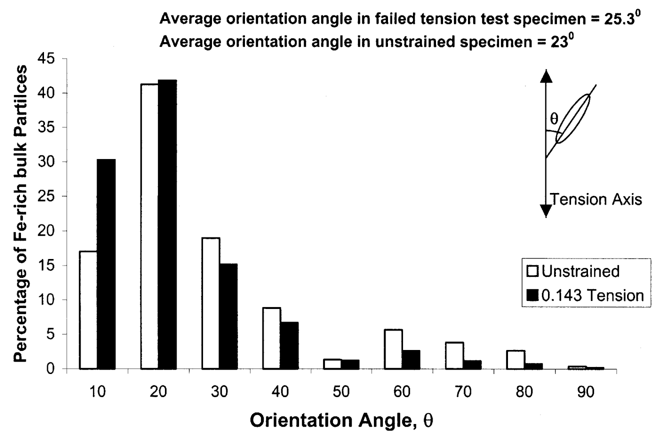

Fig. 17—Comparison of morphological orientation distribution of Fe-rich bulk intermetallic particles in unstrained specimen and the failed tensile test specimen.

Table II. Comparison of 2-D and 3-D Damage (Percent) under Uniaxial Tension

Tensile True Strain	0.037	0.072	0.107	Failed Specimen
2-D damage, f (pct)	9.25	15.1	30.1	27.1
3-D damage, F (pct)	6.3	12.2	27.75	26.2

occurred if the tensile load were applied perpendicular to the extrusion direction. The experimental data on the morphological orientation distribution supports this hypothesis. Figure 16 shows a plot of morphological orientation distribution of bulk Fe-rich gray intermetallic particles in the unstrained specimen and in the failed tensile test specimen. Observe that there are no significant differences in the two orientation distributions. For example, in the failed tensile test specimen, 87 pct of the particles are in the orientation range of 0 to 30 deg, as compared to 77 pct of the particles in this orientation range in the unstrained specimen. Therefore, it can be concluded that the particle rotations do not affect the particle cracking under tensile load significantly, when the loading direction is parallel to the axis of anisotropy. Figure 17 shows a plot of the number fraction F of cracked/broken Fe-rich particles in 3-D microstructural space, as a function of strain under uniaxial tension. Table II reports both the 2-D and 3-D number fraction of damaged particles (f and F, respectively) at the different strain levels. Observe that in these tensile test specimens, the 2-D and 3-D number fractions of the cracked particles have comparable values at each strain level studied.

The experimental data on average volume and surface area of the damaged particles and particle rotations reveal that, in uniaxial tension, more and more smaller and equiaxed particles tend to crack at higher and higher stress levels. Consequently, the average dimension of cracked particles in the direction perpendicular to the vertical metallographic plane approaches a value close to the corresponding average dimension of the overall bulk particle population. Therefore, on the average, as the strain increases, the probability of a cracked particle intersecting the chosen metallographic plane approaches the corresponding average probability for the overall bulk particle population. Consequently, as the strain increases, the fraction of cracked particles observed on the chosen metallographic plane in a given specimen also approaches to the true 3-D number fraction of cracked particles F, as observed experimentally (Table II). Therefore, in the case of tensile test specimens, when the loading direction is parallel to the axis of anisotropy (which is the extrusion axis), 2-D damage measurements provide a reasonable representation of the 3-D damage evolution, particularly at high strain levels. However, this is not true for the damage evolution in compression when the loading direction is parallel to the axis of anisotropy.

IV. SUMMARY AND CONCLUSIONS

Stereology and image analysis have been used to quantify 2-D and 3-D damage evolution (particle cracking) of Fe-rich intermetallic particles in an extruded 6061 Al-alloy. The quantitative data lead to following important observations and conclusions.

1. The relative magnitudes of the 2-D number fraction of cracked particles and the corresponding 3-D number fraction in the same specimen depend in a complex manner on particle shape, microstructural anisotropy, and relative orientation of the loading direction and axis of anisotropy. There are significant differences in the 2-D and 3-D number fraction of cracked particles at each strain level for damage evolution under compressive load applied parallel to the axis of anisotropy, and, therefore, in such cases, the 2-D damage trends can be quite deceptive. On the other hand, for damage evolution under tension when tensile load is applied parallel to the axis of microstructural anisotropy, the values of 2-D and 3-D number fraction of cracked particles are comparable, and therefore, for such a combination of type of load, loading direction, microstructural geometry, and axis of anisotropy, 2-D measurements are adequate for characterization of 3-D damage evolution under uniaxial tension.
2. Significant particle rotations take place during damage evolution under compression, when the loading direction is parallel to the axis of microstructural anisotropy (which is the extrusion axis). These particle rotations bring new larger nonequiaxed particles in the orientations that facilitate particle cracking. Therefore, the evolution of damage due to particle cracking is intimately linked with the particle rotation phenomena, and it should be incorporated in the models and theories of damage initiation due to particle cracking.
3. When compressive stress is applied in the direction parallel to the axis of anisotropy, the average volume, surface area, and orientation angle of the cracked particles *increase* with strain, as a result of the particle rotations. On the other hand, the 3-D shape factor decreases with strain, as more and more nonequiaxed particles crack at higher strains due to particle rotations.
4. When tensile stress is applied in the direction parallel to the axis of anisotropy, the average volume and surface area of the cracked particles decrease with the tensile strain, and the 3-D shape factor f cracked particles increases with strain. These trends are in agreement with the predictions of the particle cracking theories, as no significant particle rotations occur under these conditions.

ACKNOWLEDGMENTS

This research was supported through research grants from the United States National Science Foundation (Grant no. DMR-9816618) and Sandia National Laboratories (Livermore, CA) under DOE Contract No. DE-AC04-95AL85000. The financial support is gratefully acknowledged.

REFERENCES

1. R.T. DeHoff and F.N. Rhines: *Quantitative Microscopy*, McGraw-Hill, New York, NY, 1968.
2. E.E. Underwood: *Quantitative Stereology*, Addison-Wesley, Reading, MA, 1970, pp. 214-19.
3. C.V. Howard and M.G. Reed: *Unbiased Stereology*, BIOS Scientific Publishers, Oxford, United Kingdom, 1998, pp. 69-105.
4. L.M. Karlsson and L.M. Cruz Orive: *J. Microsc.*, 1992, vol. 165, pp. 391-415.
5. Jien-Wei Yeh and Wen-Pin Liu: *Metall. Mater. Trans. A*, 1996, vol. 27A, pp. 3558-69.
6. R. Doglione, J.L. Douziech, C. Berdin, and D. Francois: *Mater. Sci. Forum*, 1996, pp. 130-39.
7. E.N. Pan, C.S. Lin, and C.R. Loper: *Am. Foundrymen Soc. Trans.*, 1990, vol. 98, pp. 735-46.
8. J. Gurland and J. Plateau: *Trans. ASM*, 1963, vol. 56, pp. 442-52.
9. M.D. Dighe: Master's Thesis, Georgia Institute of Technology, 1999.
10. M.D. Dighe, A.M. Gokhale, and M.F. Horstemeyer: *Metall. Mater. Trans. A*, 2002, vol. 33A, pp. 555-65.
11. M.D. Dighe and A.M. Gokhale, and M.F. Horstemeyer: *Metall. Mater. Trans. A*, 1998, vol. 29, pp. 905-08.
12. M.D. Dighe, A.M. Gokhale, and M.F. Horstemeyer: *Metall. Mater. Trans. A*, 2000, vol. 31, pp. 1725-31.
13. A.J. Baddeley, H.J. Gundersen, and L.M. Cruz-Orive: *J. Microsc.*, 1986, vol. 142, part 3, pp. 259-76.
14. A.M. Gokhale and W.J. Drury: *Metall. Mater. Trans. A*, 1994, vol. 25A, pp. 919-29.
15. D.C. Sterio: *J. Microsc.*, 1984, vol. 134, pp. 127-36.
16. A. Tewari and A.M. Gokhale: *J. Microsc.*, 2000, vol. 200, part 3, pp. 227-83.
17. A. Tewari, A.M. Gokhale, and R.M. German: *Acta Mater.*, 1999, vol. 47, pp. 3721-34.
18. P. Louis and A.M. Gokhale: *Metall. Mater. Trans. A*, 1995, vol. 26A, pp. 1449-54.
19. A.S. Argon, J. Im, and R. Safoglu: *Metall. Trans. A*, 1975, vol. 6A, pp. 825-37.
20. J. Gurland: *Acta Metall.*, 1972, vol. 20, pp. 735-41.
21. J.L. Maloney and W.M. Garrison, Jr.: *Scripta Metall.*, 1989, vol. 23, pp. 2097-2100.
22. T.B. Cox and J.R. Low: *Metall. Trans.*, vol. 5, pp. 1457-70.